Attenuation behavior of thermoacoustic combustion instability analyzed by a complex-network- and synchronization-based approach

Shogo Murayama and Hiroshi Gotoda*

Department of Mechanical Engineering, Tokyo University of Science, 6-3-1 Niijuku, Katsushika-ku, Tokyo 125-8585, Japan

(Received 27 December 2018; revised manuscript received 1 April 2019; published 30 May 2019)

We conduct an experimental study of the attenuation behavior of thermoacoustic combustion instability from the viewpoints of complex networks and synchronization. The spatiotemporally phase-synchronized state between the vertexes in weighted networks near an injector rim is notably degenerated as thermoacoustic combustion instability is suppressed by a steady air jet issued from the injector rim. The synchronization index clearly captures the attenuation of the mutual coupling between pressure and heat release rate fluctuations. The decrease in the periodicity of noisy-periodic oscillations in a flow velocity field significantly affects the mutual coupling, resulting in the suppression of thermoacoustic combustion instability.

DOI: 10.1103/PhysRevE.99.052222

I. INTRODUCTION

The recent sophisticated methodologies of time series analysis based on the theories of dynamical systems and complex networks have made progress toward an in-depth understanding and interpretation of complex combustion dynamics. These methodologies are becoming increasingly important for the treatment of a large variety of unstable combustion phenomena including flame front instability driven by buoyancy or swirl interaction [1], radiative heat loss [2], and turbulent fire [3,4]. Thermoacoustic combustion instability, which is self-sustaining and undesirable instability in practical combustion systems, arises as a result of the strong interaction among hydrodynamics, acoustic waves, and heat release rate fluctuations [5,6]. The highly nonlinear dynamic behavior of the transition from stable combustion to thermoacoustic combustion instability and vice versa is a subject currently being focused on by the combustion community, which has adopted potential methodologies based on complex networks to extract the hidden nature in complex combustion states [7]. The Indian Institute of Technology Madras group has presented two important experimental studies [8,9] of a thermoacoustic combustion system consisting of a bluff-body-type turbulent combustor as follows: (1) the importance of the visibility graph [10] constructed from pressure fluctuations for the early detection of the onset of thermoacoustic combustion instability, involving the link between the scale-free nature and fractality during combustion noise [8], and (2) the role of a large-scale wake structure on the physical mechanism leading to thermoacoustic combustion instability using a spatial network constructed from flow velocity fluctuations [9]. Our recent experimental studies using a complex-network-based approach (the visibility graph [10], ϵ-recurrence networks [11], and turbulence networks [12]) have clarified the possible presence of scale-free and small-world structures during thermoacoustic combustion instability in a swirl-stabilized turbulent combustor, and we proposed a new detector of a precursor of thermoacoustic combustion instability [13–15]. On another front, the modeling of thermoacoustic combustion systems through synchronization theory has recently received attention [16–18]. The Kuramoto model [19], which describes the synchronized state in coupled oscillators, plays a vital role in understanding the mutual coupling between pressure and heat release rate fluctuations during thermoacoustic combustion instability in a bluff-body-type turbulent combustor [17]. Godavarthi *et al.* [20] have reported that networks constructed from both joint- and cross-recurrence plots are useful for detecting the generalized synchronization state between pressure and heat release rate fluctuations. On the basis of a study by Mondal *et al.* [17], a recent computational study [21] has shown the availability of the Kuramoto order parameter to capture a precursor of thermoacoustic combustion instability in a rocket model combustor.

Our primary interest in this study is to understand the attenuation behavior of thermoacoustic combustion instability in relation to combustion control from the viewpoints of complex networks and synchronization. Various passive and active control methods to suppress thermoacoustic combustion instability have been extensively introduced (their strategies have been summarized in some review papers [22,23]). The key point for suppressing thermoacoustic combustion instability is to alter the flame–vortex interaction so as to reduce the mutual coupling between pressure and heat release rate fluctuations inside the combustor. Secondary air injection into flame front is a potentially useful method of suppressing thermoacoustic combustion instability [24–28]. Similarly to previous studies [24–28], we adopt a steady secondary air injection system in this study. The objective of this study is to elucidate how the steady injection of a secondary air jet into the flame base alters the dynamic behavior of thermoacoustic combustion instability using advanced analytical methods based on the theories of complex networks and synchronization. As an important and fundamental case study related to thermoacoustic combustion instability in a gas-turbine combustor, we deal with the combustion dynamics in a laboratory-scale

*Corresponding author: gotoda@rs.tus.ac.jp

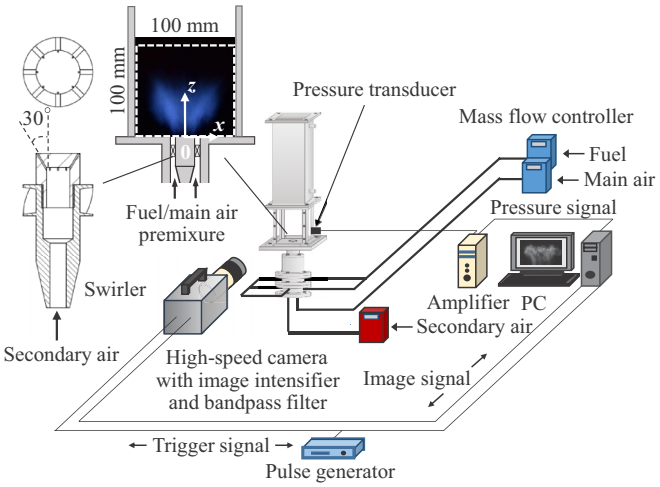

FIG. 1. Schematic of our experimental system.

swirl-stabilized turbulent combustor. In this study, we first compute the synchronization parameter [29] in terms of complex networks. We next propose a measure, the *synchronization index*, to capture the mutual coupling between pressure and heat release rate fluctuations. This measure represents the correlation between the phase synchronization parameter and the joint probability of recurrence plots constructed from two different phase spaces. Finally, we investigate the spatial distribution of the vertex strength in weighted networks constructed from a flow velocity field. This paper is structured as follows. We briefly describe the experimental system in Sec. II and the mathematical framework of our analytical methods in Sec. III. The results and discussion are given in Sec. IV, and we present a summary in Sec. V.

II. EXPERIMENTS

Figure 1 shows a schematic of our experimental system. The combustion rig is identical to that used in a previous study [15] except for an axial swirler. We consider a steady injection of a secondary air jet as an actuator to suppress thermoacoustic combustion instability. The axial swirler with the injector, which has a vane angle of 40° relative to the inlet premixture stream, is installed as a flame holder at the inlet of the combustion chamber. The injection angle of the injector is 30°, and the injector contains eight holes with a diameter of 0.6 mm. A methane-main air mixture is used as the premixture. The inlet main air at 300 K is supplied to the combustion chamber at a volume flow rate (mean axial flow velocity at the inlet of the combustion chamber) of 152.4 liters/min (6.0 m/s). The swirl number [15] of the premixture is 0.70. The initial equivalence ratio of the fuel-main air premixture ϕ without issuing the steady secondary air is set to 0.81 because it is under this condition that well-developed thermoacoustic combustion instability is formed. The steady air percentage X_a, defined as the ratio of the secondary air flow rate to the main air flow rate, is varied from 0 to 8.0%.

In this study, we simultaneously measure the pressure fluctuations p' and OH* chemiluminescence emission intensity fluctuations I'_{OH^*}. Note that the OH* chemiluminescence emission intensity is an important physical quantity that indicates the heat release rate in the study of the dynamical behavior of thermoacoustic combustion instability. p' is obtained using a pressure transducer (JTEKT Products, PD104K-10 kPa), which is placed at a distance of 20 mm from the inlet on the wall of the combustion chamber, while I'_{OH^*} is obtained using a high-speed camera (Photron, FASTCAM SA-Z) with an image intensifier (Hamamatsu Photonics, C9548-03). An OH band-pass filter (ASAHI SPECTRA Co., MZ0310) with a bandwidth of ± 2 nm centered at a wavelength of $\lambda = 310$ nm is set before the camera lens. The actual size of each image is 100 mm$\times$100 mm with a resolution of 512$\times$512 pixels. The sampling frequency of both p' and I'_{OH^*} is 6 kHz. Similarly to a previous study [15], we obtain the spatiotemporal evolution of the flow velocity field during thermoacoustic combustion instability subjected to steady secondary air injection using a high-speed particle image velocimetry (PIV) system. Details of the PIV system have been reported in Ref. [15]. As in our previous study [15], the entire flow field during thermoacoustic combustion instability subjected to steady secondary air injection predominately consists of three stable recirculation zones: an inner recirculation flow zone (IRZ), an outer recirculation flow zone (ORZ) in the dump region, and a recirculation flow zone in the wake of the center-body (RZ). These recirculation flows allow the entire flame to be maintained, with the roll up of the flame caused by vortical structures stemming from the convective interaction in the shear layer between the IRZ and the ORZ.

III. MATHEMATICAL FRAMEWORK OF ANALYTICAL METHODS

In the following subsections, we briefly describe the central ideas behind the mathematics of the methodologies based on the theories of complex networks and synchronization.

A. Synchronization parameter

The synchronization parameter [29,30] enables us to measure the synchronized state in complex networks. We apply the synchronization parameter r_l to the second-order moment of OH* chemiluminescence emission intensity fluctuations $W'_{\mathrm{OH}^*}[= \langle |I'_{\mathrm{OH}^*}(x) - \langle I'_{\mathrm{OH}^*}(x)\rangle|^2\rangle$, where $\langle\cdot\rangle$ denotes the mean over I'_{OH^*} with respect to the x direction at a constant z; see Fig. 2]. To estimate r_l, we construct weighted networks, where the nodes are each grid at location z, while the edges between the nodes are the products of the connecting strength w_{ij} and phase synchronization parameter r_{ij} values.

The determinism of cross-recurrence plots (CRPs) [31] quantifies the similarity of dynamic behavior between two trajectories in the same phase space. We estimate the determinism D_r as w_{ij} in this study. For the construction of CRPs, the temporal evolutions of $W'_{\mathrm{OH}^*,i}$ on grid i and $W'_{\mathrm{OH}^*,j}$ on grid j are first simultaneously embedded into identical d-dimensional phase spaces as $\mathbf{W}_{\mathrm{OH}^*,i}(t) = [W'_{\mathrm{OH}^*,i}(t), W'_{\mathrm{OH}^*,i}(t+\tau), \ldots, W'_{\mathrm{OH}^*,i}(t+(d-1)\tau)]$ and $\mathbf{W}_{\mathrm{OH}^*,j}(t) = [W'_{\mathrm{OH}^*,j}(t), W'_{\mathrm{OH}^*,j}(t+\tau), \ldots, W'_{\mathrm{OH}^*,j}(t+(d-1)\tau)]$, where τ is the embedding delay time. The cross-recurrence matrix $\mathbf{C}$ is defined as

$$\mathrm{C}_{m,n} = \Theta(\epsilon - ||\mathbf{W}_{\mathrm{OH}^*,i}(t_m) - \mathbf{W}_{\mathrm{OH}^*,j}(t_n)||), \qquad (1)$$

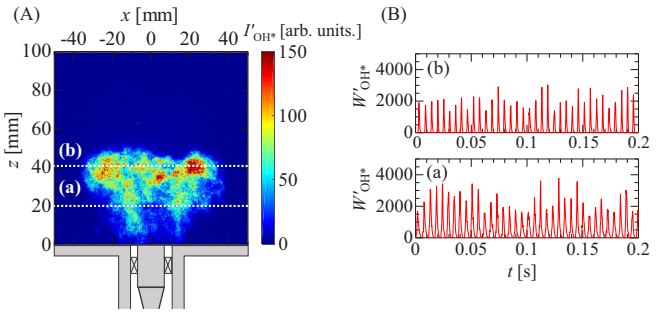

FIG. 2. (A) Instantaneous OH^* chemiluminescence emission intensity image and (B) the extracted temporal evolution of the second-order moment of OH^* chemiluminescence emission intensity fluctuations W'_{OH^*} during thermoacoustic combustion instability at (a) $z = 20$ mm and (b) $z = 40$ mm.

where Θ is the Heaviside function, ϵ is the threshold, $||\cdot||$ is the Euclidean norm, and m and n are arbitrary point in the trajectories in d-dimensional phase space. D_r signifies the time distance τ' from the main diagonal line and is computed separately for each diagonal line parallel to the main diagonal line ($m = n$) as follows:

$$D_r(\tau') = \frac{\sum_{l=l_{\min}}^{N-\tau'} l P_{\tau'}(l)}{\sum_{l=1}^{N-\tau'} l P_{\tau'}(l)}. \tag{2}$$

Here, N is the number of phase space vectors, $P_{\tau'}(l)$ is the frequency distribution of length l of each diagonal line parallel to the main diagonal line, and $l_{\min}$ is the shortest allowable diagonal line length (= 5). We set ϵ so as to satisfy a recurrence rate of R_r $(= \frac{\sum_{m,n} C_{m,n}}{N^2}) = 0.05$ and τ' is set to the value for which D_r takes a maximum.

The phase synchronization parameter r_{ij}, which quantifies the degree of phase synchronization between $W'_{OH^*,i}$ and $W'_{OH^*,j}$, is defined as

$$r_{ij} = \left| \lim_{\Delta t \to \infty} \frac{1}{\Delta t} \int_t e^{i[\theta_i(t') - \theta_j(t')]}\, dt' \right|, \tag{3}$$

where Δt is the time interval, and $\theta_i(t')$ and $\theta_j(t')$ are instantaneous phases of $W'_{OH^*,i}$ and $W'_{OH^*,j}$, respectively, obtained by the Hilbert transformation [32]. Here, r_{ij} takes a value from 0 to 1, and $r_{ij} = 1$ corresponds to the phase synchronization.

We define the adjacency matrix as

$$A_{ij} = \begin{cases} w_{ij} r_{ij} & i \neq j \\ 0 & i = j \end{cases}. \tag{4}$$

The value of r_l, corresponding to the average value of nodes in weighted networks, is obtained as

$$r_l = \frac{1}{2N_l} \sum_i \sum_j w_{ij} r_{ij}, \tag{5}$$

where N_l is the number of edges, r_l ranges from 0 to 1, and $r_l = 1$ corresponds to a completely synchronized state. The node strength $\mathbf{s}$ is given as $s_i = \sum_j w_{ij} r_{ij}$.

B. Synchronization index

We propose a parameter, the synchronization index, to detect the significant changes in mutual coupling between pressure and heat release rate fluctuations. It considers the phase synchronization parameter and the joint probability of recurrence plots [31] constructed from two different phase spaces. The phase synchronization parameter r_{pq} is defined as

$$r_{pq} = \left| \lim_{\Delta t \to \infty} \frac{1}{\Delta t} \int_t e^{i[\theta_p(t') - \theta_q(t')]}\, dt' \right|, \tag{6}$$

where $\theta_p(t')$ and $\theta_q(t')$ are the instantaneous phases of p' and W'_{OH^*}, respectively, to quantify the degree of phase synchronization between p' and W'_{OH^*}. To estimate the joint probability of recurrence plots, J_r, we construct the joint recurrence matrix $\mathbf{J}$ as

$$\begin{aligned} \mathrm{J}_{m,n} &= \Theta(\epsilon - ||\mathbf{p}(t_m) - \mathbf{p}(t_n)||) \\ &\quad \times \Theta(\epsilon - ||\mathbf{W}_{OH^*}(t_m) - \mathbf{W}_{OH^*}(t_n)||), \end{aligned} \tag{7}$$

where $\mathbf{p}(t) = [p'(t), p'(t+\tau), \ldots, p'(t+(d-1)\tau)]$ and $\mathbf{W}_{OH^*}(t) = [W'_{OH^*}(t), W'_{OH^*}(t+\tau), \ldots, W'_{OH^*}(t+(d-1)\tau)]$ are d-dimensional phase space vectors of p' and W'_{OH^*}, respectively. J_r, representing the ratio of common parts in each recurrence plot, is obtained as

$$J_r = \frac{M - R_r}{1 - R_r}, \tag{8}$$

$$M = \frac{\frac{1}{N^2} \sum_{m,n}^{N} \mathrm{J}_{m,n}}{R_r}. \tag{9}$$

J_r ranges from 0 to 1, where $J_r = 1$ corresponds to the state of general synchronization. The synchronization index S_I is defined as

$$S_I = J_r \times r_{pq}. \tag{10}$$

S_I increases with the strength of the mutual coupling between pressure and heat release rate fluctuations. A recent experimental study [33] using a swirl-stabilized turbulent combustor has shown the presence of period-doubling bifurcation during thermoacoustic combustion oscillations. Note that in our preliminary test using a nonlinear dynamical system [34,35] that produced period-doubling bifurcation, we confirmed the validity of the synchronization index through comparison with the computed S_I and J_r.

IV. RESULTS AND DISCUSSION

Figure 3 shows the power spectrum distribution of the sound pressure level p_s and the standard deviation of pressure fluctuations p'_{rms} in terms of the secondary air percentage X_a at equivalence ratio $\phi = 0.81$. p'_{rms} monotonically decreases with increasing X_a. It abruptly decreases to approximately 0.01 kPa at X_a of 6.5%. Thermoacoustic combustion instability with a dominant frequency of approximately 170 Hz, which corresponds to the 1/4 acoustic mode in the longitudinal direction of the combustor, is observed in the power spectrum at $X_a \leqslant 6.0\%$. The amplitudes of thermoacoustic combustion instability are significantly reduced while retaining slight periodicity. When X_a exceeds 6.5%, the dominant peak of the pressure

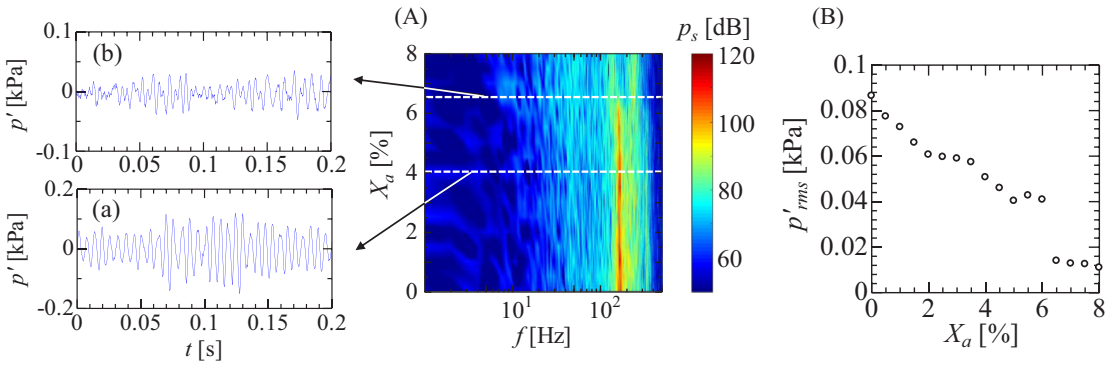

FIG. 3. (A) Power spectrum distribution of sound pressure level p_s and temporal evolution of pressure fluctuations p' at secondary air percentages X_a of (a) 4.0% and (b) 6.5%. (B) Variation in the standard deviation of pressure fluctuations p'_{rms} as a function of X_a.

spectrum nearly disappears, and the spectrum consists of a broad frequency band with small-amplitude fluctuations. A secondary air injection of 6.5% allows the formation of thermoacoustic combustion instability to be markedly suppressed.

Figure 4 shows the spatial distributions of the vertex strength s and synchronization parameter r_l in the weighted networks constructed from the second-order moment of OH* chemiluminescence emission intensity fluctuations W'_{OH^*} as functions of X_a and vertical location z. We observe high s in the region 5 mm $\leqslant z \leqslant$ 45 mm at $X_a = 0\%$. The range of high s remains nearly unchanged at $X_a \leqslant 4.0\%$ and abruptly vanishes at $X_a \geqslant 6.5\%$. A similar trend is observed in r_l. Gómez-Gardeñes *et al.* [29] reported that the phase-synchronized state expands as r_l is increased. On this basis, it is presumed that strongly correlated vertexes during thermoacoustic combustion instability are formed in the region from near the injector rim to the shear layer between the IRZ and the ORZ, identifying the formation of a spatiotemporally phase-synchronized state. An important observation here is the gradual decrease in s at $z = 14$ mm near the flame base. This indicates that steady secondary air injection acting on the oscillating flame base, causing a change in the convective vortical structures, results in the disappearance of the spatiotemporal phase synchronization. The suppression of thermoacoustic combustion instability is associated with the disappearance of the spatiotemporal phase synchronization.

The spatial distribution of the synchronization index S_I between pressure fluctuations p' and the second-order moment of OH* chemiluminescence intensity fluctuations W'_{OH^*} is shown in Fig. 5 as functions of X_a and z. At $X_a = 0\%$, S_I takes a high value in the range of 10 mm $\leqslant z \leqslant$ 40 mm, revealing the driving regime of thermoacoustic combustion instability. Note that in our preliminary test, the region of high S_I corresponds to that with a strongly positive pseudo-Rayleigh index. S_I gradually decreases when X_a exceeds approximately 3.0% and abruptly becomes almost zero at $X_a \geqslant 6.5\%$. This means that a significant unbounded interaction between p' and W'_{OH^*} occurs at $X_a \geqslant 6.5\%$. These results show that the synchronization index proposed in this study enables us to successfully capture the gradual attenuation of thermoacoustic combustion instability, extracting the driving region of thermoacoustic combustion instability. Note that in our preliminary test, the spatial distribution of J_r as a function of X_a and z does not sufficiently correspond to that of the Rayleigh index, which means that the joint probability of recurrence is not always sufficient for dealing with the interaction between pressure and heat release rate fluctuations. It is also important to emphasize that the synchronization index ranges from zero to unity. The Rayleigh index is sensitive to the amplitudes of pressure and heat release rate fluctuations, and does not range from zero to unity. In these contexts, the synchronization index is more suitable for treating the

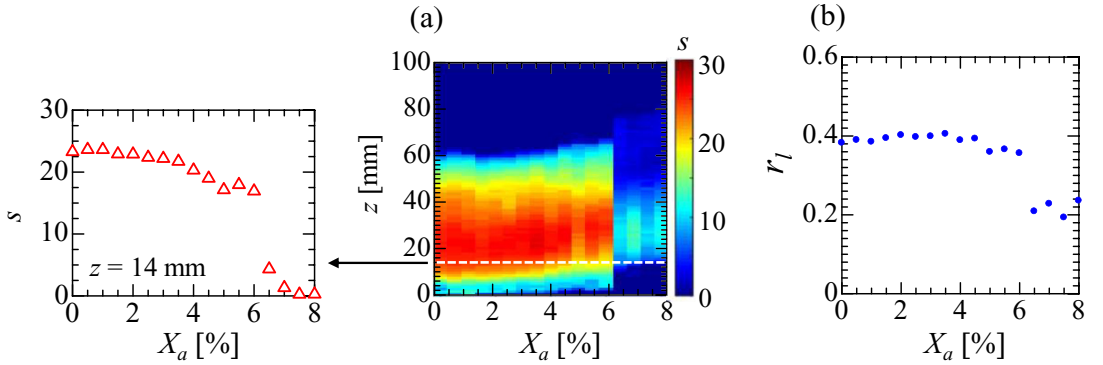

FIG. 4. (a) Spatial distribution of vertex strength s constructed from the second-order moment of OH* chemiluminescence emission intensity fluctuations W'_{OH^*} as a function of the secondary air percentage X_a and location z. (b) Variation in synchronization parameter r_l constructed from W'_{OH^*} as a function of X_a.

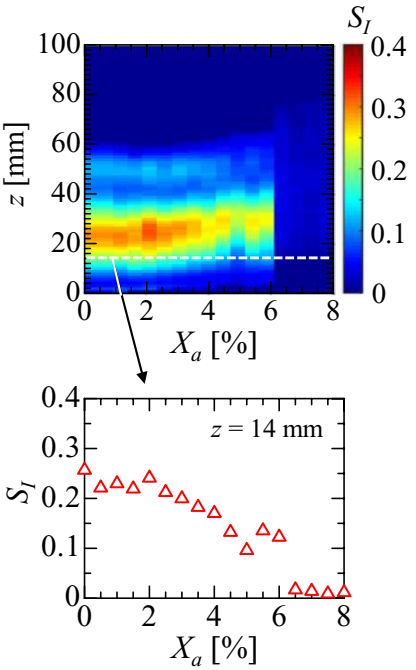

FIG. 5. Spatial distribution of the synchronization index S_I between pressure fluctuations p' and the second-order moment of OH* chemiluminescence intensity fluctuations W'_{OH^*} as a function of the secondary air percentage X_a.

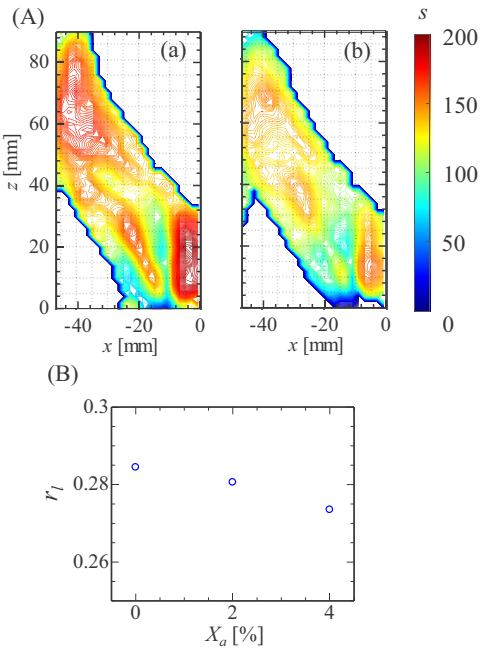

FIG. 6. (A) Spatial distribution of vertex strength s in the weighted networks constructed from flow velocity fluctuations u' at secondary air percentages X_a of (a) 0% and (b) 4.0%. (B) Synchronization parameter r_l in the weighted networks constructed from u' as a function of X_a. The analytical region is from the injector rim to the shear layer, and the vertexes correspond to each grid.

interaction between pressure and heat release rate fluctuations than the Rayleigh index and the joint probability of recurrence.

Figure 6 shows the spatial distribution of s and the variations in r_l for flow velocity fluctuations u' at $X_a = 0$ and 4.0%. Here, s at $X_a = 0\%$ takes high values at the wake of the center body. It significantly decreases when X_a is 4.0%. We observe a slight decrease in r_l with increasing X_a, indicating a decrease in the strength of the spatiotemporally phase-synchronized state in the flow velocity field. The spatial distribution of s for the reconstructed flow velocity fluctuations obtained by the detail coefficient of the discrete wavelet transformation [36,37], representing the near-dominant frequencies of thermoacoustic combustion instability, is shown in Fig. 7 for different X_a values. As in a previous study [37], we use the wavelet multiresolution technique in this study. Here, s at $X_a = 0\%$ takes high values in both the wake of the center body and the flame base. It significantly decreases with increasing X_a, showing clear degeneration of the spatiotemporally phase-synchronized state in the flow velocity field.

Our recent study [15] using the multiscale complexity-entropy causality plane has shown that noisy periodic oscillations appear in local flow velocity fluctuations along a streamline from near the injector rim to the shear layer between the IRZ and the ORZ during thermoacoustic combustion instability. We here examine the dynamic behavior of a flow velocity field subjected to secondary air injection by estimating the spatial distribution of the permutation entropy H_p and the Jensen–Shannon statistical complexity C_{JS} in terms of the embedding delay time τ (see Ref. [15] for details of the computation of both measures). Note that C_{JS} is defined as the product of H_p and Q_{JS}, where Q_{JS} is the disequilibrium of the probability distribution in the permutation patterns, and the dynamical states can be classified in relation to the degree of complexity into noisy periodic oscillations, noisy chaos, and stochastic fluctuations on the basis of the shape of the simultaneous distributions of H_p and C_{JS} as a function of τ. Variations in H_p and C_{JS} of the second-order moment of flow velocity fluctuations W'_u are shown in Fig. 8 as functions of τ and z at $X_a = 0\%$ and 4.0%. Here, $W'_u = \langle |u'(x) - \langle u'(x)\rangle|^2\rangle$, $u' = (u'_x{}^2 + u'_z{}^2)^{1/2}$, and $u'_x(u'_z)$ is the flow velocity fluctuations in the $x(z)$ direction. At $X_a = 0\%$, both H_p and

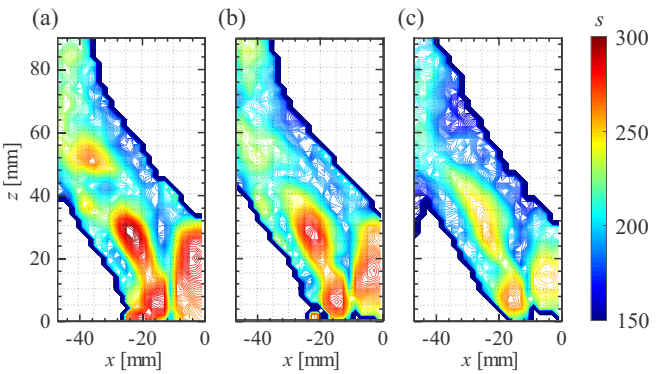

FIG. 7. Spatial distribution of vertex strength s of reconstructed flow velocity fluctuations using detail coefficient of discrete wavelet transformation, representing the near-dominant frequencies of thermoacoustic combustion instability, at secondary air percentages X_a of (a) 0%, (b) 2.0%, and (c) 4.0%.

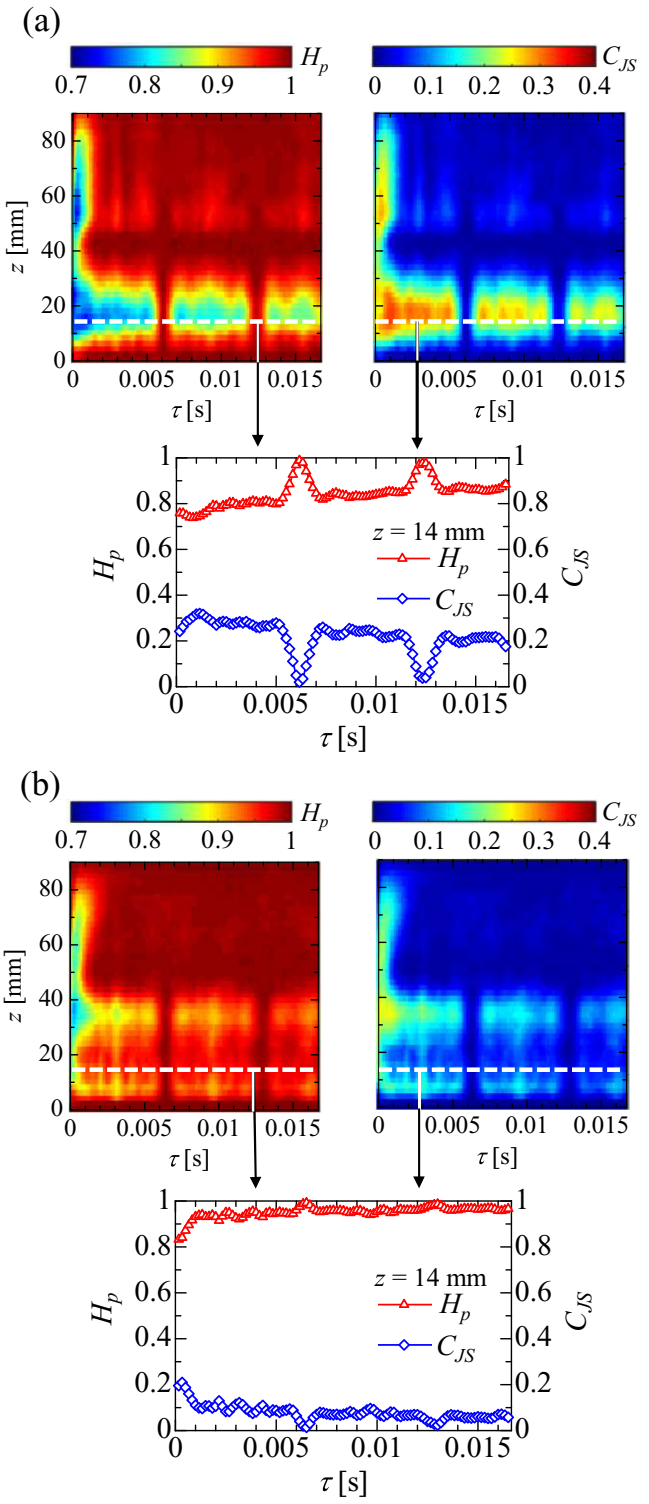

FIG. 8. Variations in the permutation entropy H_p and Jensen−Shannon statistical complexity C_{JS} of the second-order moment of flow velocity fluctuations W_u' as functions of embedding delay time τ and vertical location z at secondary air percentages X_a of (a) 0% and (b) 4.0%.

C_{JS} for W_u' at $z = 14$ mm, corresponding to the flame base, periodically change in terms of τ, corresponding to the main period of thermoacoustic combustion instability. On the basis of a previous study [15], the dynamic behavior of the flow

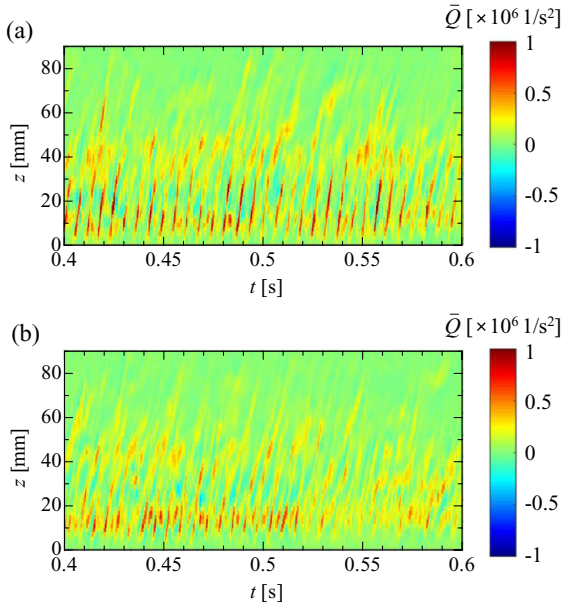

FIG. 9. Temporal evolution of average value of the second invariant of velocity gradient tensor $\bar{Q}$ with respect to x in terms of vertical location z at secondary air percentages X_a of (a) 0% and (b) 4.0%.

velocity field near the flame base represents noisy periodic oscillations equivalent to the dynamics of a stochastically driven van der Pol oscillator. When X_a exceeds 4.0%, the periodic local maximum (minimum) of H_p (C_{JS}) starts to disappear during steady secondary air injection. This clearly shows that secondary air injection reduces the formation of noisy periodic oscillations in the flow velocity field. H_p near the flame base takes high values when X_a is 4.0%, which means that the randomness of the dynamic behavior is increased by secondary air injection. The formation of a stabilized flame due to the impingement of a high-momentum air jet allows the periodicity of thermoacoustic combustion instability to degenerate. This accentuates the irregular component with a small magnitude inherently included in flow velocity fluctuations, resulting in the appearance of distributions with high permutation entropy near the flame base under steady secondary air injection. The temporal evolution of the average value of the second invariant of the velocity gradient tensor $\bar{Q}[= \langle \frac{1}{2}(|\Omega|^2 - |S|^2)\rangle$, where $\Omega = \frac{\partial u_x}{\partial z} - \frac{\partial u_z}{\partial x}$ and $S = \frac{\partial u_x}{\partial z} + \frac{\partial u_z}{\partial x}]$, with respect to x is shown in Fig. 9 in terms of z at $X_a = 0\%$ and 4.0%. $\bar{Q}$ periodically takes high positive values with time at 5 mm $\leqslant z \leqslant$ 35 mm, corresponding to the region from near the injector rim to the shear layer between the IRZ and the ORZ. However, the region with the periodic formation of a high $\bar{Q}$ becomes narrow when X_a is 4.0%, showing the suppression of the generation of periodically convecting vortices downstream. In addition to a finding reported by Sato *et al.* [26], on the basis of the results obtained from the multiscale complexity–entropy causality plane and the spatiotemporal changes in the second invariant of the velocity gradient tensor, the periodicity of noisy periodic oscillations forming the spatiotemporally phase-synchronized state in the flow velocity field starts to be lost as X_a substantially increases. The degeneration of the periodicity due to the interaction between the high-momentum air jet

and the vortices shed from the injector rim and the possible local dilution of the premixture in the flame base weakens the mutual coupling between pressure and heat release rate fluctuations, resulting in the attenuation of thermoacoustic combustion instability. In this study, we have analyzed the attenuation behavior of thermoacoustic combustion instability subjected to steady secondary air injection from the viewpoints of complex networks and synchronization. The obtained findings are expected to help understand the suppression process of combustion instability related to combustion control in thermoacoustic systems.

V. SUMMARY

We have experimentally studied the attenuation behavior of thermoacoustic combustion instability in a swirl-stabilized turbulent combustor using a complex-network- and synchronization-based approach. The spatiotemporally phase-synchronized state between the vertexes in weighted networks near an injector rim is notably degenerated as thermoacoustic combustion instability is suppressed by a steady air jet issued from the injector rim. This is reasonably identified using the synchronization parameter. The synchronization index proposed in this study clearly captures the attenuation of the mutual coupling between pressure and heat release rate fluctuations in thermoacoustic combustion instability. The periodicity of noisy periodic oscillations in a flow velocity field is lost by the strong impingement of a steady secondary air jet into the flame base. The decrease in the periodicity significantly affects the mutual coupling, resulting in the suppression of thermoacoustic combustion instability.

ACKNOWLEDGMENTS

H.G. was supported by a Grant-in-Aid for Scientific Research (B) 16H04284 and 19H02085. We thank Mr. Hayato Todoroki (Photron Co.) for helping us use the high-speed video camera (Photron, FASTCAM SA-Z) employed in this study. We would like to express our thanks to Souta Nakano and Takuya Kurosaka (Tokyo University of Science) for their support of our experiments.

[1] H. Gotoda, H. Kobayashi, and K. Hayashi, Phys. Rev. E **95**, 022201 (2017).
[2] H. Kinugawa, K. Ueda, and H. Gotoda, Chaos **26**, 033104 (2016).
[3] K. Takagi, H. Gotoda, T. Miyano, S. Murayama, and I. T. Tokuda, Chaos **28**, 045116 (2018).
[4] K. Takagi and H. Gotoda, Phys. Rev. E **98**, 032207 (2018).
[5] *Combustion Instabilities in Gas Turbine Engines: Operational Experience, Fundamental Mechanisms, and Modeling*, edited by T. C. Lieuwen and V. Yang, Progress in Astronautics and Aeronautics Vol. 210 (American Institute of Aeronautics and Astronautics, Reston, VA, 2005).
[6] T. C. Lieuwen, *Unsteady Combustor Physics* (Cambridge University Press, Cambridge, 2012).
[7] M. P. Juniper and R. I. Sujith, Annu. Rev. Fluid Mech. **50**, 661 (2018).
[8] M. Murugesan and R. I. Sujith, J. Fluid Mech. **772**, 225 (2015).
[9] V. R. Unni, A. Krishnan, R. Manikandan, N. B. George, R. I. Sujith, N. Marwan, and J. Kurths, Chaos **28**, 063125 (2018).
[10] L. Lacasa, B. Luque, F. Ballesteros, J. Luque, and J. C. Nuño, Proc. Natl. Acad. Sci. USA **105**, 4972 (2008).
[11] R. V. Donner, M. Small, J. F. Donges, N. Marwan, Y. Zou, R. Xiang, and J. Kurths, Int. J. Bifurcation Chaos **21**, 1019 (2011).
[12] K. Taira, A. G. Nair, and S. L. Brunton, J. Fluid Mech. **795**, R2 (2016).
[13] Y. Okuno, M. Small, and H. Gotoda, Chaos **25**, 043107 (2015).
[14] H. Gotoda, H. Kinugawa, R. Tsujimoto, S. Domen, and Y. Okuno, Phys. Rev. Appl. **7**, 044027 (2017).
[15] S. Murayama, H. Kinugawa, I. T. Tokuda, and H. Gotoda, Phys. Rev. E **97**, 022223 (2018).
[16] Y. Guan, M. Murugesan, and L. K. B. Li, Chaos **28**, 093109 (2018).
[17] S. Mondal, V. R. Unni, and R. I. Sujith, J. Fluid Mech. **811**, 659 (2017).
[18] N. B. George, V. R. Unni, M. Raghunathan, and R. I. Sujith, J. Fluid Mech. **849**, 615 (2018).
[19] Y. Kuramoto, *Chemical Oscillations, Waves, and Turbulence* (Dover, New York, 2003).
[20] V. Godavarthi, S. A. Pawar, V. R. Unni, R. I. Sujith, N. Marwan, and J. Kurths, Chaos **28**, 113111 (2018).
[21] T. Hashimoto, H. Shibuya, H. Gotoda, Y. Ohmichi, and S. Matsuyama, Phys. Rev. E **99**, 032208 (2019).
[22] S. Candel, Proc. Combust. Inst. **29**, 1 (2002).
[23] A. P. Dowling and A. S. Morgans, Ann. Rev. Fluid Mech. **37**, 151 (2005).
[24] J. H. Uhm and S. Acharya, Combust. Flame **139**, 106 (2004).
[25] J. H. Uhm and S. Acharya, Combust. Flame **142**, 348 (2005).
[26] H. Sato, M. Ikame, K. Harumi, T. Kishi, K. Hiraoka, H. Oka, A. K. Hayashi, and S. Ogawa, JSME Intl. J. B **48**, 328 (2005).
[27] J. H. Uhm and S. Acharya, Combust. Flame **147**, 22 (2006).
[28] H. M. Altay, D. E. Hudgins, R. L. Speth, A. M. Annaswamy, and A. F. Ghoniem, Combust. Flame **157**, 686 (2010).
[29] J. Gómez-Gardeñes, Y. Moreno, and A. Arenas, Phys. Rev. Lett. **98**, 034101 (2007).
[30] R. Gutiérrez, A. Amann, S. Assenza, J. Gómez-Gardeñes, V. Latora, and S. Boccaletti, Phys. Rev. Lett. **107**, 234103 (2011).
[31] N. Marwan, M. C. Romano, M. Thiel, and J. Kurths, Phys. Rep. **438**, 237 (2007).
[32] S. Balusamy, L. K. B. Li, Z. Han, M. P. Juniper, and S. Hochgreb, Proc. Combust. Inst. **35**, 3229 (2015).
[33] D. Noh, E. Karlis, S. Navarro-Martinez, Y. Hardalupas, A. M. K. P. Taylor, D. Fredrich, and W. P. Jones, Proc. Combust. Inst. **37**, 5333 (2019).

[34] K. Takagi and H. Gotoda, 69th Annual Meeting of the APS Division of Fluid Dynamics, Bull. Am. Phys. Soc. (APS) **61** (2016).

[35] S. Mondal, A. Mukhopadhyay, and S. Sen, Combust. Theory Model. **21**, 487 (2017).

[36] S. G. Mallat, IEEE Trans. Acoustics Speech Signal Proc. **37**, 2091 (1989).

[37] Q. An, W. Y. Kwong, B. D. Geraedts, and A. M. Steinberg, Combust. Flame **168**, 228 (2016).